Spring 5-6-2024

Investigating Murine Uterine Tissue Dynamics: Biomechanical and Histological Perspectives on Postpartum Involution and Scar-Induced Remodeling

Savannah Elizabeth Chatman
Washington University – McKelvey School of Engineering

WASHINGTON UNIVERSITY IN ST. LOUIS

McKelvey School of Engineering
Department of Biomedical Engineering

Thesis Examination Committee:
Matthew R. Bersi, Chair
Christine O'Brien
Michelle Oyen

Investigating Murine Uterine Tissue Dynamics: Biomechanical and Histological Perspectives on Postpartum Involution and Scar-Induced Remodeling

by

Savannah Elizabeth Chatman

A thesis presented to
the McKelvey School of Engineering
of Washington University in
partial fulfillment of the
requirements for the degree
of Master of Science

May 2024
St. Louis, Missouri

Table of Contents

List of Figures

Acknowledgments

I would first like to start by thanking my parents, Lori and Gary Chatman. You have both blessed me with endless opportunities to explore all my interests and challenge my worldview. There is not a world where I discover my love for engineering and women's health without you sending me to engineering camps and pushing me to get out of my comfort zone. To my grandfathers, Gary Sr. And Ivory, thank you for always showing up for me and being there to listen when I needed you. I would also like to thank my lovely brothers, Justin and Joshua. Your support, advice, laughter, and hugs are the foundation that has allowed me to grow and blossom into the person I am.

To Ashleigh, Chandler, Christine, and Grace, your friendships have been inspirational and growing up with you was the greatest gift I could ask for. You all challenged me at every step of my education and continuously tasked me with becoming the best version of myself. Thank you for allowing me to be my craziest self as that has allowed me to always go after what I want.

To my Scripps girls, your creativity, grace, intellect, and confidence played an integral role in leading me to where I am today. You all pushed me to truly follow my dreams and continuously show me that anything is possible.

To my Westgate family, thank you for making St. Louis such a home for me. You guys supported me through one of my hardest seasons and helped propel me into the best times of my life. We've seen so much of the world together, and I can't wait to keep learning from you.

To Chase, thank you for all of your support over the past year and for being my rock throughout this process. You make every journey special.

Last, but most certainly not least, I would like to thank Dr. Bersi. You have served as an incredible mentor and guiding force as I took on this project. Thank you for all that you've taught me so far and all you have to teach me in the future. To Niyousha and Abigail, I've learned so much from both of you, and thank you for all your help in moving this work forward. To all the members of the Soft Tissue Mechanics Lab, thank you for being an amazing group of people to work with.

Savannah Elizabeth Chatman

Washington University in St. Louis

May 2024

For Cha-Che. I couldn't have done any of this without you.

ABSTRACT OF THE THESIS

Investigating Murine Uterine Tissue Dynamics: Biomechanical and Histological Perspectives on Postpartum Involution and Scar-Induced Remodeling

by

Savannah Elizabeth Chatman

Master of Science in Biomedical Engineering

Washington University in St. Louis, 2024

Professor Matthew Bersi, Chair

During pregnancy, the uterus undergoes structural and mechanical transformations to withstand the demands of a successful delivery. In cases where vaginal birth is not feasible, a Cesarean section (c-section), which involves a transverse abdominal incision, is used to facilitate delivery of the fetus and placenta[1]. Following the procedure, the uterus and abdominal tissue are carefully sutured to support postpartum recovery, leading to uterine scarring at the incision site[1,2]. Understanding the relationship between uterine scar integrity, postpartum involution, and the biomechanics of uterine tissue is a crucial step toward predicting the risk of uterine rupture during future labor events. This project aims to utilize ex-vivo mechanical testing and noninvasive imaging techniques to investigate the relationship between the structure and composition of remodeled uterine tissue after the introduction of a uterine scar or after postpartum involution in female mice. Murine uterine ring samples will be used to assess the structural and mechanical properties of the uterus, with the objective of quantifying the change in biomechanical properties throughout the different uterine healing processes. Imaging techniques such as Optical Coherence Tomography (OCT) and immunohistological staining will provide insights into tissue structure. Ultimately, this project aims to unveil the connection between uterine involution, scar healing, and uterine tensile strength.

Chapter 1: Introduction

Throughout the journey of pregnancy, the uterus undergoes a series of intricate yet substantial structural and mechanical transformations that are essential for a successful delivery. These adaptations are paramount in ensuring the uterus can withstand the considerable biomechanical stresses imposed during delivery. In situations where vaginal delivery is not safe or feasible, a Cesarean section (commonly referred to as c-section) is used to deliver the fetus. -section is a surgical procedure that first involves either a transverse or longitudinal incision across the mother's abdomen to provide access to the uterus and fetus[1]. A second set of incisions is then made on the uterus in order to remove the fetus and placenta. Following delivery, the incisions are closed, and a wound healing process ensues that ultimately results in the formation of a uterine scar[1]. This form of delivery is highly invasive yet common in the United States, with one in three deliveries occurring this way. C-section delivery is typically employed when there is a risk to either the mother's or fetus's health, if the fetus is improperly positioned, if labor is not progressing safely, or if there are problems with the placenta[1]. However, women who have previously undergone delivery by C-section face an increased risk of uterine rupture when attempting vaginal births in subsequent pregnancies[2]. Uterine rupture, a rare yet critical peripartum complication, is characterized by the mechanical failure of the uterine wall either during gestation or delivery. Factors such as multiple prior c-sections and single-layer uterine closure can elevate the likelihood of this occurrence due to reduced tissue integrity and improper healing at uterine incision sites. Leveraging the structural similarities between the human and mouse uterus, herein murine uterine tissue serves as invaluable model for studying the structural and mechanical phenomena associated with remodeling of the uterus under different surgical and biological conditions.

By harnessing this comparative approach across species, the aim of this thesis is to delineate the biomechanical characteristics of uterine tissue throughout two different remodeling processes: baseline postpartum involution and scar healing post-hysterotomy (i.e., introduction of scar in nulliparous mice). The main objective of this study is to evaluate the biomechanical response of mouse uterine tissue throughout these different remodeling conditions under controlled uniaxial loading. Ultimately, this study aims to enhance our understanding of uterine biomechanics and mechanobiology, while offering potential insights into the management and prevention of complications associated with childbirth, with a specific focus on uterine rupture in women with a history of c-sections.

1.1 Uterine Structure and Function

The uterus is the primary female reproductive organ responsible for gestational development of an embryo into a fetus during pregnancy[3]. This muscular organ is in the lower abdomen and pelvis and has three main layers. The *perimetrium* is the outermost uterine layer and acts as a protective layer against tissue overstretching; the *myometrium* consists of smooth muscle cells that facilitate contractions during childbirth and the *endometrium* is a thin, vascularized mucosal layer that goes through dynamic structural changes during the menstrual cycle[3]. Each layer plays an essential role in the three major functions of the uterus. During *menstruation*, the endometrial layer is shed due to a decrease in estrogen and progesterone hormonal levels during the uterine menstrual cycle [3]. During *pregnancy*, the uterus undergoes hypertrophy, hyperplasia, and mechanical stretching for 36 weeks after embryo implantation to accommodate growth of the fetus throughout gestation[4]. During *delivery* and active labor, the cervix dilates alongside strong uterine smooth muscle contractions in the myometrium due to an increase in oxytocin and prostaglandins; this positive feedback loop facilitates successful vaginal delivery[4]. As a

consequence of these different functions and biological mechanisms, the uterus undergoes different types of remodeling to return to its baseline (homeostatic) structure.

1.1.1 Principles Behind Uterine Remodeling

Proper uterine remodeling is necessary for maternal health, fetal development, and successful delivery. The process of uterine remodeling is facilitated through physiological changes in the extracellular matrix and uterine vasculature within each layer of the uterus[5]. While the endometrium cyclically remodels during the menstrual cycle to prepare for possible embryo implantation, the entire organ undergoes significant growth and remodeling during pregnancy and throughout postpartum involution. These three biological processes are regulated through hormonal changes that influence resident cell behaviors and signal for different immune cell populations (e.g., macrophages) to respond and alter uterine matrix structure and organization[5]. Each cell type acts in a coordinated fashion to facilitate and stimulate growth, regeneration, vascular repair, and angiogenesis that is required for proper remodeling of the uterus. During pregnancy, the uterus undergoes a more in-depth transformation to support attachment and growth of the placenta to the maternal vasculature. The placenta delivers maternal blood to the fetus via the aorta, uterine arteries, spiral arteries, and radial arteries, thus creating a change in the hemodynamics and physiology of the uterine vascular system[5]. These changes are facilitated by the mechanobiological response of fetal trophoblasts, immune cells, and vascular smooth muscle cells[6]. Indeed, dynamic uterine remodeling is essential for the overall physiological function of the uterus and for preventing maternal and reproductive health challenges including endometriosis, eclampsia, pre-eclampsia, and fetal growth restriction.

1.1.2 Postpartum Involution

Postpartum involution is the process of returning the uterus to a state where it can support another pregnancy after parturition[6,7]. Implantation and placentation lead to significant changes in the uterine structure, specifically with regard to vascular remodeling. Arterial remodeling is necessary to support the changes in blood flow required to develop the placenta and support the growing fetus[9]. There is also a thickening of the endometrial lining as well as an increase in the size of the uterus[11]. Because pregnancy increases the weight, amount of extracellular matrix components (e.g., collagen and elastin), cell count, and overall size of the uterus in order to accommodate the necessary physiological changes to the uterine structure and vasculature, it is essential for this tissue to undergo substantial reverse remodeling to return the tissue back to its non-pregnant state[8]. While complete reversal of the tissue after parturition likely does not occur, this process of involution is facilitated through hormonal stimulation – specifically the withdrawal of estrogen and progesterone levels post birth – and the degradative response of uterine macrophages to remove excess cells and extracellular matrix[10,13]. Myometrial smooth muscle cells, along with collagenase and other proteolytic enzymes, also aid in this process by compressing the newly formed uterine vasculature to return the tissue to its pre-pregnancy size[11]. This vasoconstriction helps to accelerate the involution process since autolysis and infarction of uterine blood vessels, creating an inflammatory environment that works to decrease the overall size of the organ[13]. Ultimately, these structural and physiological changes to the uterus allow the body to support multiple pregnancies[11].

1.1.3 Effects of a Cesarean Section on the Uterus

In cases where vaginal delivery is not possible, the fetus will be delivered via C-section. This is one of the most common surgical procedures performed in the United States, with rate of over

32% of all births[14]. This form of delivery is accomplished by creating an abdominal incision to access the uterus, followed by a hysterotomy to provide access to the fetus[12]. The transverse uterine incision goes through all three layers of the wall, allowing for the successful delivery of both the fetus and placenta. This procedure poses many risks to both the mother and the fetus, including an elevated risk of blood loss, surgical injury, and post-surgical uterine rupture at the incision site[14]. After surgery, the subsequent scar remodeling, combined with the ongoing process of postpartum involution, should allow for the uterus to accommodate the tissue's biomechanical demands. However, there are currently no reliable methods to non-invasively determine uterine scar integrity and strength of the healing incision site. The uterine wound healing process begins with inflammation in the area of the damaged blood vessels due to the immune system's reaction to the surgery[15]. The subsequent stages of proliferation and maturation allow for collagen formation and remodeling at the incision site along with granulation and neovascularization to support reoxygenation and recellularization in the area of injury[15]. These processes are assisted via signaling of various growth factors such as TGF-β, CTGF, bFGF, and VEGF, that ultimately support the remodeling and healing of each of the three layers of the uterus[15]. Notwithstanding this coordinated wound healing response, the introduction of the uterine scar following c-section combined with the effects of gestation and contraction in subsequent pregnancies may alter the tissue's structure in a way that compromises its overall biomechanical integrity thereby posing a risk to overall maternal health[16].

Ineffective healing of Cesarean section scars can lead to future reproductive health complications, including uterine rupture. Uterine rupture involves a partial or total division of the three layers of the uterus, allowing for parts of the fetus, amniotic fluid, or umbilical cord to enter the peritoneal cavity[17]. This life-threatening injury can lead to extreme maternal blood loss and

potential loss of the fetus[10]. While the risk of this complication is rare during traditional vaginal deliveries, women having had at least one c-section are at an increased risk of uterine rupture when attempting labor in subsequent deliveries[18]. The increased uterine rupture risk suggests that c-section scar remodeling and postpartum involution may weaken the overall tissue integrity resulting in compromised biomechanical properties.

1.1.4 Animal Model for Different Postpartum Conditions

Mouse models are a useful way to research the mechanisms underlying different postpartum conditions because of their short gestation time. Mice and humans share a similar layered uterine structure and parturition cascade, including an increase in contractile proteins like oxytocin receptor, prostaglandin F-2-alpha receptor, and connexin-43 at term[19]. The labor and delivery process of both species also shares key components. Although there are key physiological differences across species, including a difference in estrogen and progesterone regulation throughout pregnancy as well as a difference in the shape (humans have a single uterus whereas mice have bifurcated uterine horns) and number of offspring (humans tend to have singleton pregnancies while mice birth litters), mouse models allow for an inexpensive way to understand certain mechanobiological mechanisms that result from uterine remodeling associated with pregnancy, c-section scar formation, and postpartum involution.

1.2 Scope of Thesis

The primary objective of this thesis is to employ ex-vivo mechanical testing alongside noninvasive imaging techniques to comprehensively explore the relationship between uterine scar morphology, postpartum involution, and the strength of uterine tissue against rupture. This research aims to characterize the structural and biomechanical properties of the mouse uterus during postpartum

involution while also delineating a correlative relationship between the extent of uterine scar healing/regeneration and tensile strength.

1.2.1 Aim 1 – Characterize the Relationship Between Uterine Scar Healing and Tensile Strength

This objective aims to elucidate the intricate relationship between uterine scar healing/regeneration and its impact on the tensile strength of the tissue. Uterine horns undergoing recovery from hysterotomy will be subjected to cyclic uniaxial loading and extension-to-failure tests. Imaging modalities such as Optical Coherence Tomography (OCT) and immunofluorescent staining will facilitate the examination of alterations in tissue microstructure. Assessment of these tissues will be conducted at intervals of 1, 2, and 3 weeks post-hysterotomy.

1.2.2 Aim 2 – Explore Alterations in the Structure and Biomechanics of the Mouse Uterus during Postpartum Involution

This objective entails investigating changes in the tensile strength of uterine horns in wild-type mice at various stages of postpartum involution. Biomechanical properties will be assessed through cyclic uniaxial loading and extension-to-failure tests. Utilizing OCT and immunoflurescent staining, alterations in tissue microstructure will be examined. Evaluation of tissue microstructure and biomechanics will be conducted at intervals of 1, 3, 7, and 14 days postpartum.

Chapter 2: Methodology

The project utilizes a uniaxial tensile testing procedure and data analysis pipeline for mouse uterine ring tissue using the ElectroForce 3200 Mechanical Testing System. All collected data will be analyzed in MATLAB such that the changes in deformation, stress, strain, stretch, and geometry are identified.

Prior to performing mechanical testing, each sample was imaged using OCT to understand the longitudinal tissue structure. Each sample also underwent histological and immunohistochemical staining for elastin, αSMA, uterine natural killer (NK) cells, macrophages, collagen, and other cellular components that may be contributing to the reverse remodeling and restoration of uterine dimensions throughout postpartum involution.

To characterize the structure and biomechanics of mouse uterine tissue during postpartum involution, wild-type mice 1,3, 7, and 14 days after natural delivery were utilized. To understand the relationship between uterine scar healing and uterine tensile strength, uterine horns from wild-type mice were analyzed 1, 2, and 3 weeks after hysterotomy was performed.

2.1 Surgical Model of Uterine Scarring - Hysterotomy Procedure

Non-pregnant female wild-type mice (C57BL/6J) were anesthetized using sterile surgical technique prior to midline incision and externalization of one uterine horn. Two 3-5 mm longitudinal uterine incisions were introduced and subsequently closed with 6/0 absorbable suture prior to sterile washing and closure of the abdominal cavity. After the uterus and abdomen were closed, animals were allowed to recover for 1, 2, or 3 weeks before euthanasia.

2.2 Animal Model for Postpartum Involution

Timed-pregnant wild-type mice were purchased (The Jackson Laboratory) and allowed to deliver naturally. The animals were then euthanized at either 1, 3, 7, or 14 days after delivery to allow for assessment of postpartum involution at different time points.

2.3 Uniaxial Testing Materials and Equipment

The experimental procedure used to mechanically load a mouse uterine ring sample was developed and performed on the ElectroForce 3200 Series III Test Instrument (TA Instruments)[20]. The experimental setup, along with a detailed schematic of the required components, is described in **Figure 1** (sample mounting fixtures and PBS bath) and **Figure 2** (complete setup with cameras). The two mounting fixtures, shown in **Figure 1**, function as adjustable two-sided grips that allow the mounted sample to be axially stretched by the machine. A suture travels through the U-shaped attachment piece (denoted U-piece) of both mounting fixtures and through the bottom bars at both ends, with the sample mounted in between the two U-pieces. By altering the position of the U-piece, varying levels of tension can be applied to the sample. The nuts on the mounting fixture allow for adjustment of the U-piece such that the screws do not interfere with the nut and provide optimal camera viewing once the sample is mounted and placed in the ElectroForce system.

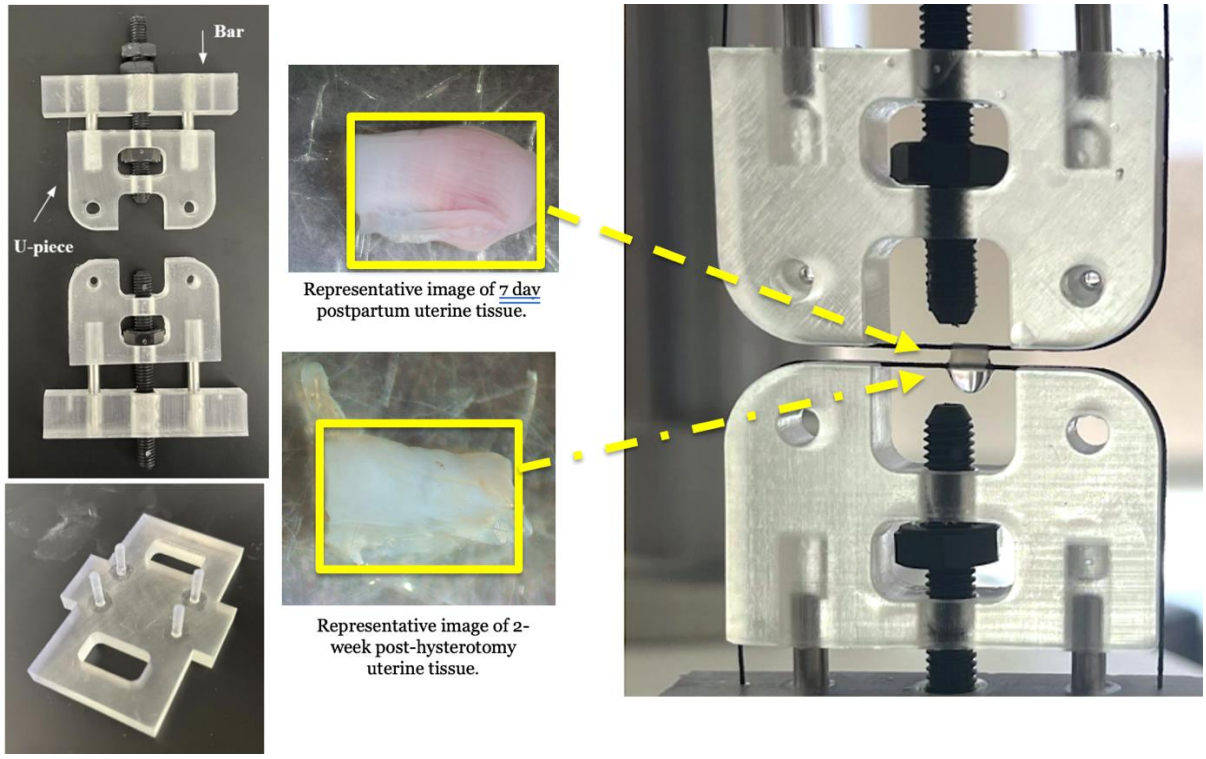

Figure 1: Components required for proper testing of mouse uterine ring samples on the ElectroForce 3200 machine, including the mounting pieces, uterine ring samples, and the adjustable mounting fixtures with the uterine ring sample mounted and ready for testing (from left to right).

2.3.1 Uniaxial Testing Mounting Procedure and Setup

To properly mount the ring-shaped sample of uterine tissue, a 2-0 silk suture is measured so that it is about 15 inches long and can secure on one of the adjustable fixtures. Each end of the suture was first threaded through openings on the same end of each bottom bar (see **Figure 1**) and double knotted to secure the suture in place. Uterine horn samples were then prepared by submerging the entire murine uterine sample in 1X phosphate buffer saline (PBS). With the sample in a petri dish, an approximately 3.5 mm section of the horn was cut to create a ring for mechanical testing. With angled tweezers threaded through the ring sample, the suture was threaded through the inner lumen of the sample. The position of the uterine ring was then adjusted along the suture until it was centered over the black screw of the adjustable fixtures to ensure proper positioning for the mechanical test. Once the sample was centered, the suture was cut and secured at both open

ends of the appropriate bottom bars with a double knot. Each nut was tightened to remove slack in the suture passing through the uterine ring sample; in this way, each piece of suture was continuous along one of the individual adjustable fixtures. The mounted sample and mounting plate were then submerged in a 1X PBS bath at 4°C for at least 2 hours prior to testing to allow for tissue equilibration after handling.

To perform mechanical testing on the ElectroForce 3200 machine, an adapter must be added to the top adjustable fixture and secured to the force transducer on the machine (up to a maximum force of 45 N). The orientation of the mounted sample was adjusted so that it was positioned at a 135/45° angle relative to the front of the machine to allow for optimal camera placement and viewing during the test. After properly positioning the fixtures and mounting plate on the force transducer, the height of the machine's stage was adjusted so the mounting apparatus on the ElectroForce crosshead could securely connect to the bottom adjustable fixture with a screw threaded tightly through the PBS bath. A circular light was placed under the PBS bath on the stage to allow for illumination and clear viewing of the sample from the perpendicular cameras. Once the sample apparatus – the two adjustable fixtures containing the sample in an empty PBS bath – was properly set up, the height of the ElectroForce actuator was adjusted and approximately 400 mL of 1X PBS was added to the bath to hydrate the sample. After ensuring no fluid leakage from any part of the sample apparatus, two cameras were attached to the stage and positioned such that one was facing the tissue directly and the other was 90° from the front. An example of tissue sample captured from both camera angles can be seen in **Figure 2B**. The view settings on both cameras were adjusted (zoom, focus, aperture, etc.) for optimal recording within a custom-built LabView image acquisition software. The full experimental setup is shown in Figure 2B.

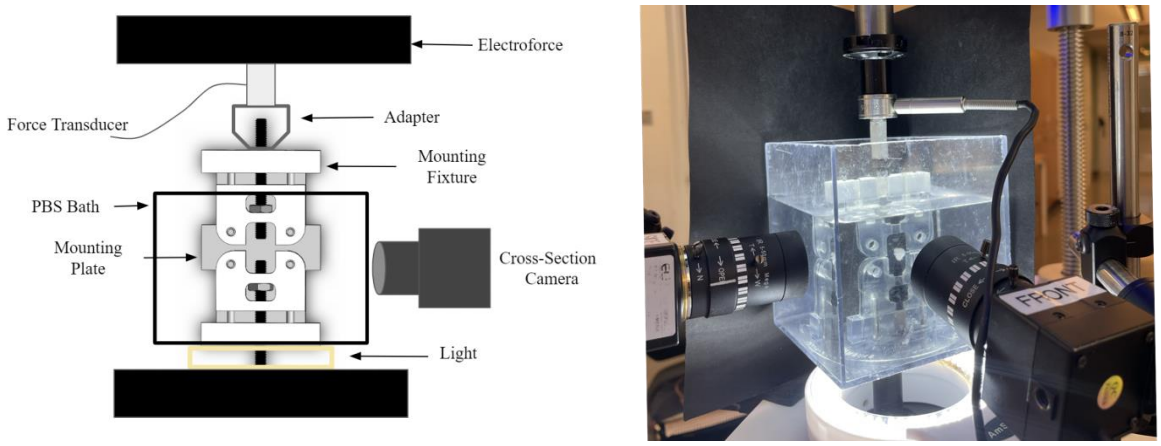

Figure 2: A) Detailed schematic outlining all components needed for proper testing of uterine ring samples. B) Complete experimental test setup with cameras and mouse uterine ring sample mounted in the ElectroForce 3200 machine.

2.3.2 Uniaxial Testing Procedure

A preload of 0.01 N was set prior to testing to establish a reference position for the entire mechanical testing procedure. After defining this equilibrium position, four cyclic loads were applied to the sample. The prescribed loads were chosen to be 0.1 N, 0.3 N, 0.5 N, and 0.7 N. These numbers were selected to ensure the highest likelihood that samples would not experience mechanical failure prior to the end of the mechanical test. Each load/unload cycle was performed with a dwell time of 400 seconds to allow the tissue to return close to its equilibrium position before the next ramp begins. The applied displacement for each load was increased at a rate of 0.1 mm/s, and each of the prescribed load cycles was repeated in duplicate before the prescribed load level was increased. After all load cycles were completed, the sample was ramped until failure[20]. To allow for optimal analysis of the video recorded data from Labview, a checkerboard calibration tool was used to establish the video's scaling based on the current camera settings.

2.3.3 Uniaxial Testing Analysis

During the testing procedure, the force-displacement data output by the ElectroForce system was recorded in a .csv file. The software recorded the force applied to the sample via the force

transducer as well as the displacement of the ElectroForce stage at a rate of ten data points per second during each ramp phase and two data points per second during each dwell period. The force-displacement data with respect to time along with the stress-strain cycles of the ElectroForce was then plotted using MATLAB. To compare the data recorded by the ElectroForce to the video recorded data, a calibration picture was used to establish the correct scale for proper understanding of the sample geometry. Using a calibration tool with a checkerboard of 1 mm per square, the calibration factor of pixels per millimeter recorded by each of the cameras was determined. After proper calibration, the change in height of the sample throughout the test during each frame was measured by the maximum difference between the top and bottom of the sample based on the contrast in pixel intensity values. These pixel values were then converted to millimeters using the reference calibration, giving us the sample heights as recorded in real time using the camera. To analyze the mechanical properties of the tissue, the video-recorded values were used to compare the sample heights recorded by the ElectroForce during testing as well as to generate the stress-strain curve for each load cycle until failure, as seen in Figure 3.

Estimating the geometry of the sample as a rectangular prism, for simplicity, the stress experienced by the uterine ring was calculated using the Cauchy Stress described in Equation (1), where F is the measured force and A is the current cross-sectional area.

$$\sigma = F / \mathrm{A} \tag{1}$$

As previously stated, the force F was collected directly by the ElectroForce software. The reference cross-sectional area A was calculated as in Equation (2)

$$A = \mathrm{w} \times \mathrm{l} \tag{2}$$

where W and L are the width and length of the tissue sample, calculated using the calibrated LabView recorded videos. To analyze the mechanical behavior of the tissue, the stress was plotted with respect to the linear strain and stretch as described in Equation (3) and (4).

$$\epsilon = \mathrm{d}H / \mathrm{H} \tag{3}$$

$$\lambda = h / H \tag{4}$$

H is the original height of the sample while h is the current height of the tissue and dH is the change in height as measured by either the ElectroForce or recorded on the cameras via LabView. When testing to failure, the failure point was defined as the configuration with the maximum stress experienced by the sample prior to a persistent decrease in measured force.

2.4 Noninvasive Imaging

Noninvasive imaging via Optical Coherence Tomography (OCT) and immunohistological analysis was performed to assess changes in murine uterine tissue structure at each time point.

2.4.1 Optical Coherence Tomography

OCT imaging was performed on intact uterine horns using the ThorLabs Ganymede Series OCT System (930 nm; GAN611C1) prior to separating the tissue into ring samples for mechanical testing. This technique was used to analyze changes in the uterine tissue in its postpartum or post-hysterotomy conditions. For OCT imaging, the murine uterine horn was placed in a petri dish with 1X PBS. The horn was positioned so that the hysterotomy scar was facing toward the camera, if applicable. After adjusting the focus of the device to the appropriate level, longitudinal images were captured of each sample.

2.4.2 Histological Analysis

A non-mechanically tested section of the uterine horn, including a section with the scar if applicable, was prepared for sectioning and staining. Samples were embedded in Tissue-Plus™ O.C.T. Compound (PANTeK Technologies, 23-730-571) at -80°C prior to cryosectioning along the circumferential direction at an 8 µm section thickness (NX50 CryoStar).

For immunostaining, O.C.T was removed by washing in 1X PBS, and sections were fixed/permeabilized using a combined 10% neutral buffered formalin (Millipore Sigma, HT501128) and 0.1% Triton-X (Sigma-Aldrich, x100) solution. After fixation and permeabilization, sections were submerged in PBS before blocking in a solution of 5% bovine serum albumin (Sigma-Aldrich, A3059) and 5% goat serum (Sigma-Aldrich, G9023) in PBS for 1 hour at room temperature. Samples were then stained at room temperature with a primary antibody against murine tropoelastin exons 6-17 (1:300 for 4 hours) or polyclonal rabbit IgG (1:300 for 4 hours) followed by a mixture of Cy5 secondary antibody (Adam, ab6564) and conjugated αSMA-Cy3 monoclonal antibody (Millipore Sigma, C61918) (both at 1:300 for 1 hour). Stained samples were placed under a gentle rocking in PBS for 30 mins. Finally, samples were mounted in Prolong Gold with DAPI (Invitrogen, P36935) and immunofluorescent images were acquired on an Olympus DP80 dual-sensor CCD camera using a 20x magnification objective. All images were acquired with the same exposure settings for consistent visual comparison.

Quantification of elastin, collagen, macrophage (CD68+), and smooth muscle cell (αSMA+) area fraction analysis was performed using the image processing capabilities of FIJI (NIH).

For collagen staining, a Picrosirius Red staining kit (ab150681) was employed. After washing the sections in 1X PBS, adequate amounts Picrosirius Red Solution was used to cover the entire section. Incubated for 60 minutes. The slides were then rinsed twice in Acetic Acid Solution, followed by with absolute alcohol. After dehydrating the sections using absolute alcohol, the slides were mounted in synthetic resin.

Chapter 3: Results

The cyclic force-displacement data generated by the ElectroForce system was plotted over time for each sample. The tissue displacement as well as the resulting deformations in the sample's length, height, width and area over the uniaxial testing procedure were determined using the video captured by the perpendicular cameras in LabView. To characterize the mechanical properties of the mouse uterine tissue, stress-strain and stress-stretch curves for each load/unload cycle were created using the video-calculated displacement and the applied load from the ElectroForce. Representative images of the tissue during the test as well as the cyclic force-displacement data, changes in tissue deformation, displacement over time, and the Cauchy stress-stretch response can be seen in **Figure 3**.

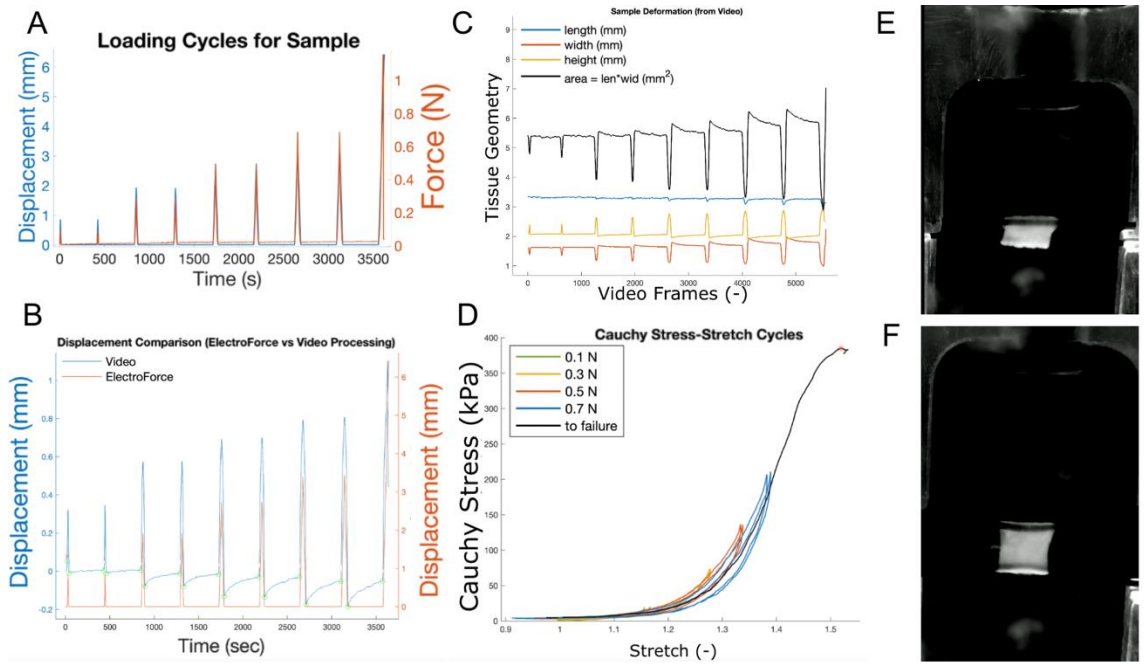

Figure 3: Representative mechanical testing results from the ElectroForce 3200 system A) Cyclic force-displacement data measured by the ElectroForce B) Comparison between the uterine ring's vertical displacement measured by the ElectroForce and the calibrated video C) Changes in the tissue's length, height, width, and area throughout the uniaxial loading test as measured by the calibrated video D) the resulting Cauchy stress and stretch experienced by the uterine ring sample. E,F) Representative images of the uterine ring sample as recorded in Labview during dwell and during the failure test.

3.1 Characterization of the Biomechanical Effect of Hysterotomy on Murine Uterine Tissue

The hysterotomy procedure and resulting scar remodeling altered the overall uterine tissue microstructure. As shown in **Figure 4**, the tomographic images at each time point (1 week, 2 week, and 3 weeks) reveal areas where the injury is beginning to close. At 1 week post-hysterotomy, there is a visible gap where the incision was made in the tissue. As the tissue continues to remodel, the 2 week post-hysterotomy tissue has areas where the tissue has begun to heal and come back together, but still has areas that have yet to heal. At 3 weeks, the tissue has healed and the scar is no longer visible.

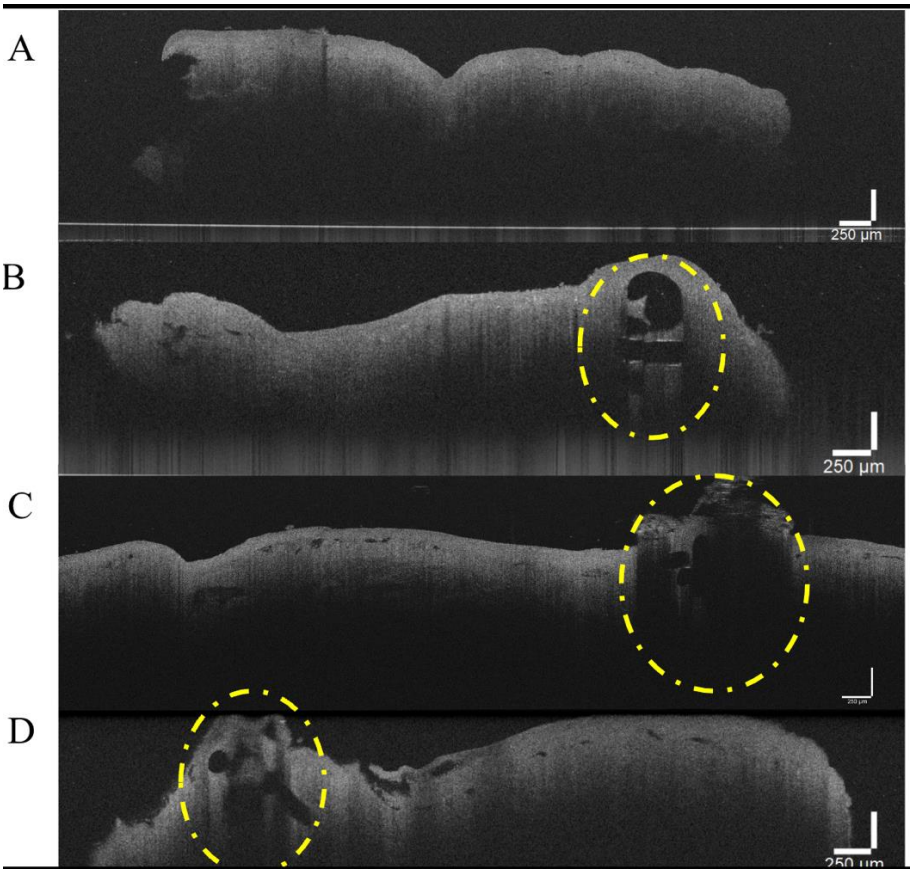

Figure 4: Representative OCT images from each time point, highlighting changes in the overall uterine tissue structure. OCT images of 8-week-old virgin uterine horns A) without surgery, B) 1 week post-hysterotomy, C) 2 weeks post-hysterotomy, and D) 3 weeks post-hysterotomy. Yellow circle indicates scar site.

These same microstructural changes are evident in the immunohistological images, shown in Figure 5. Regions where the scar is present appear acellular thereby highlighting the injury's effect of the tissue's microstructure at each time point. This is especially noticeable in the 1-week post-hysterotomy tissue. As the wound closes and heals, the smooth muscle cells of the myometrium and the uterine elastin fibers help facilitate the remodeling process. Macrophages also play a critical role in facilitating scar remodeling, with a heavier presence in the myometrium of the 1-week post-hysterotomy tissue when compared to the 3 weeks. The collagen content also changes as a result of the procedure. As seen in **Figure 7**, the collagen becomes more organized and densely pack around the injury site. After three weeks of remodeling, the organized fibers are heavily present in the endometrium, further highlighting how the tissue's microstructure changes during this process.

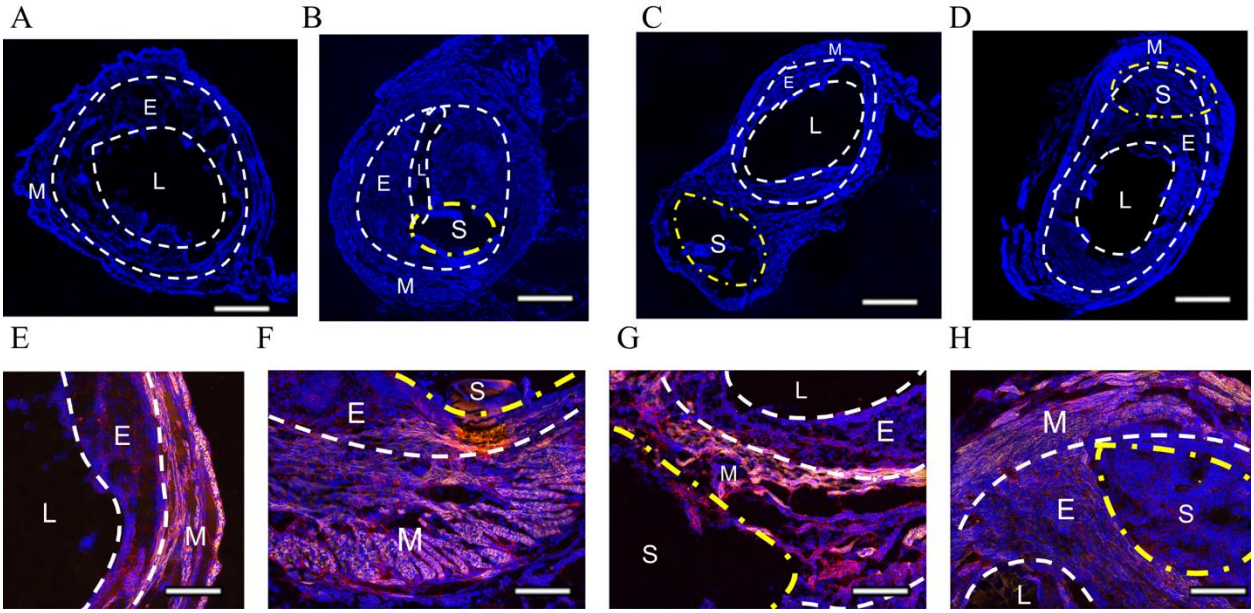

Figure 5: Representative immunofluorescence images from each time point, highlighting changes in the overall tissue's elastin (red) and smooth muscle cell (yellow) content. Immunofluorescent images of 8-week-old virgin uterine horn A,E) without surgery, B,F) 1 week post-hysterotomy, C,G) 2 weeks post-hysterotomy, and D,H) 3 weeks post-hysterotomy. Scale bars are 60 µm (Blue = DAPI, Red = elastin, yellow = smooth muscle cells); (M = Myometrium, E = Endometrium, L = Lumen, S = Scar site)

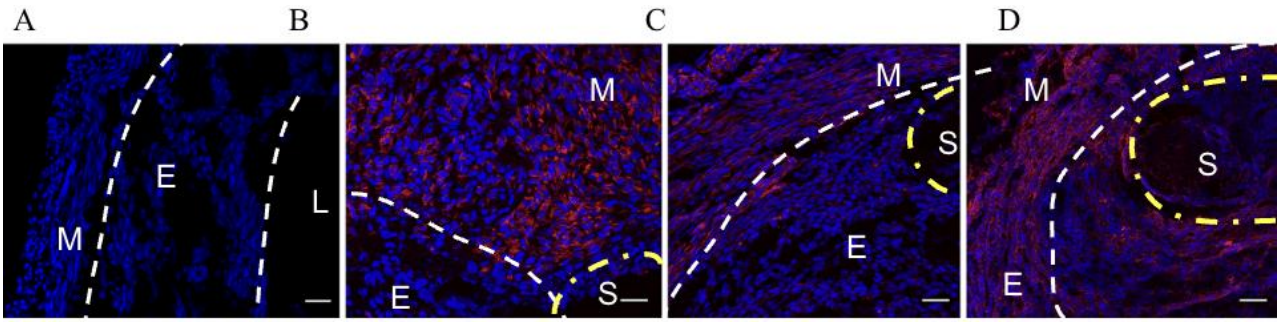

Figure 6: Representative histological images from each time point, highlighting changes in the macrophage (CD68+) content. Immunofluorescent images of 8-week-old virgin uterine horn A) without surgery B) 1 week post-hysterotomy, C) 2 weeks post-hysterotomy, and D) 3 weeks post-hysterotomy. Scale bars are 60 µm. (Blue = DAPI, Red = CD68+, macrophages); (M = Myometrium, E = Endometrium, L = Lumen, S = Scar site)

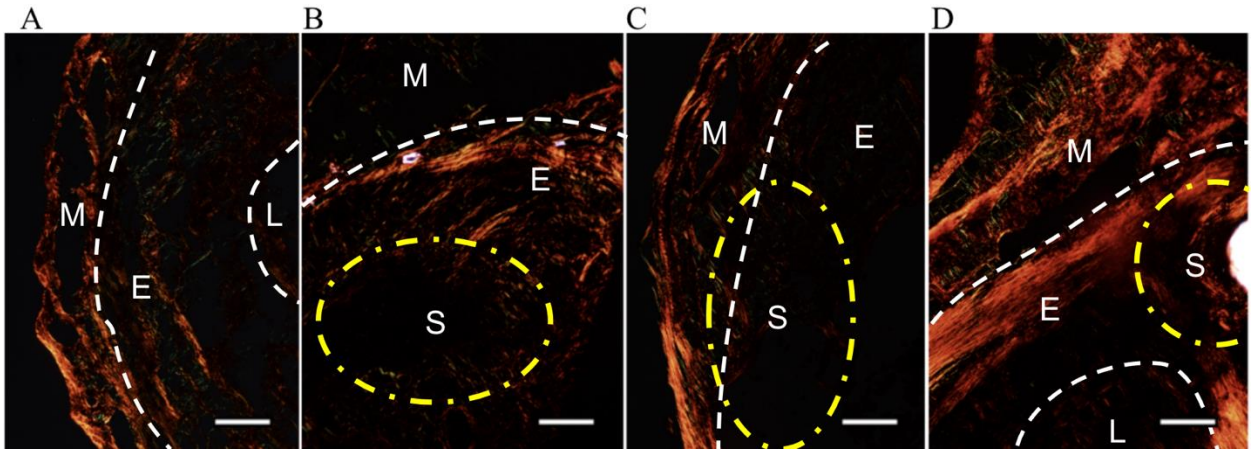

Figure 7: Representative histological images from each time point, highlighting changes in the overall tissue's collagen cell content. Birefringence images of 8-week-old, virgin uterine horn A) without surgery, B) 1 week post-hysterotomy, C) 2 weeks post-hysterotomy, and D) 3 weeks post-hysterotomy. Scale bars are 60 µm. (M = Myometrium, E = Endometrium, L = Lumen, S = Scar site)

The changes in the uterine tissue's microstructure manifest as a change in the biomechanical properties in response to uniaxial loads. When performing the uniaxial strength test, there was a difference in its response to the cyclic loads and resulting rupture force after hysterotomy. As shown in **Figure 8A**, after one-week post-hysterotomy, the murine uterine tissue ruptured at an average applied tensile force of 0.8 N, whereas the uninjured tissue ruptured at an average tensile force of 1.2 N. Over the course of remodeling, the tissue's strength begins to return such that by 3 weeks post-surgery, an applied load of 1.3 N is needed to rupture the tissue. The resulting Cauchy stress, shown in **Figure 8C**, follows this same pattern, with the tissue being able to withstand lower

amounts of stress at one week compared to three weeks post-hysterotomy. This is especially highlighted in the tissue's stress-stretch response at 0.5 N, shown in **Figure 8F**. However, the tissue's ability to withstand deformations resulting from the applied loads changes in response to the hysterotomy procedure. Over the course of remodeling, the level of strain the tissue can withstand decreases post-injury, as shown in **Figure 8D**.

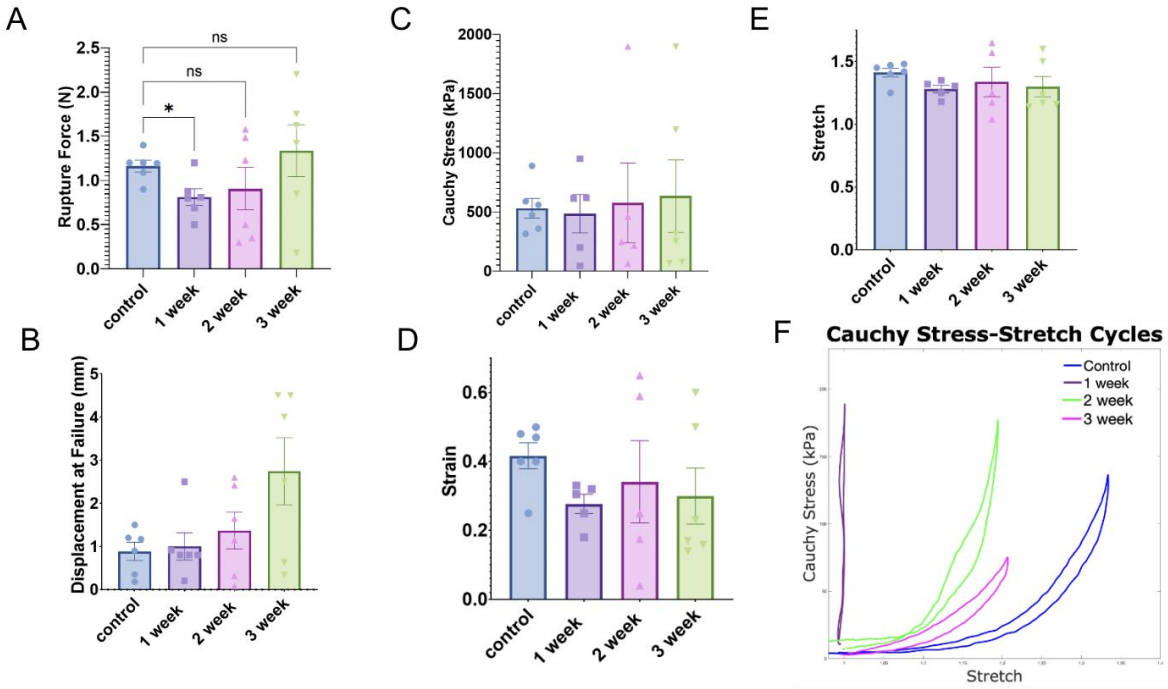

Figure 8: Uniaxial biomechanical analysis of murine uterine tissue after scar formation showing changes in A) maximum rupture force, B) maximum displacement, C) Cauchy stress at failure, D) engineering strain at failure, and E) stretch at failure. F) Representative comparison of the control, 1 week, 2 week, and 3 week post-hysterotomy Cauchy Stress-Stretch behavior as it is loaded to 0.5 N. * $p < 0.05$; Brown-Forsythe ANOVA with post-hoc Dunnett comparison to control

Overall, the hysterotomy procedure alters the uterine tissue's architecture, thus leading to changes in its biomechanical properties.

3.2 Exploration of Structural and Biomechanics Changes in Postpartum Murine Uterine Tissue

Postpartum involution also alters the structure and biomechanical response of uterine tissue. The microstructural changes in the tissue are highlighted in the OCT and immunohistological images shown in **Figure 9 and 10**. The tomographic images show the changes in the myometrium and general uterine structure over the time course of postpartum involution. As shown in **Figure 9**, the myometrium appears more vascular at 3 and 7 days postpartum but begins to return to its non-pregnant size and vascular structure by 14 days postpartum. The increase in vasculature is further highlighted in the immunohistology images. As shown in **Figure 10**, there is an increase in the elastin content at 1 day and 3 days postpartum. However, while the 7 day and 14 day postpartum tissue may have less elastin than the earlier days of postpartum involution, its content is still higher than that of the virgin tissue. There is also an increase in the number of smooth muscles cells in the myometrium at 1 day postpartum, but the content begins to return to its baseline levels after 7 days postpartum. This is shown by the red (elastin) and yellow (smooth muscle) staining in **Figure 10**. The macrophage content also increases during postpartum involution, with the 1 and 3 day postpartum tissue having a larger presence of macrophages than the control, as shown in **Figure 11**. Involution also alters the presence of collagen in the uterine tissue. Specifically, endometrial and myometrial collagen content after one and three days postpartum 1 and day 3 appears more organized and tightly pack than the collagen content in these regions by seven and fourteen days postpartum. This is highlighted in **Figure 12.**

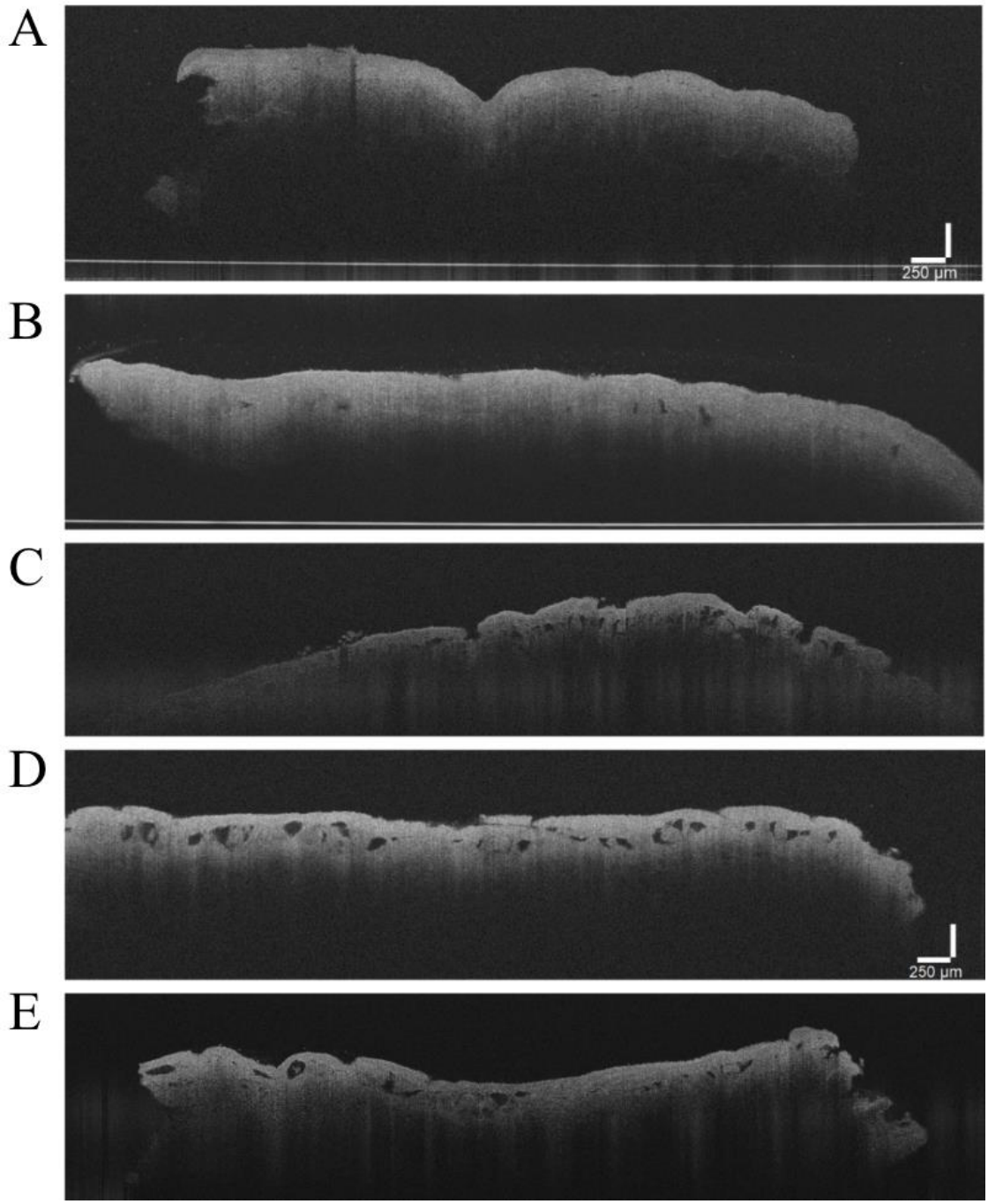

Figure 9: Representative OCT images from each postpartum time point, highlighting changes in the overall tissue structure. Longitudinal OCT images of A) 8-week-old virgin uterine horn and uterine tissue at B) 1 day, C) 3 days, D) 7 days, and E) 14 days postpartum.

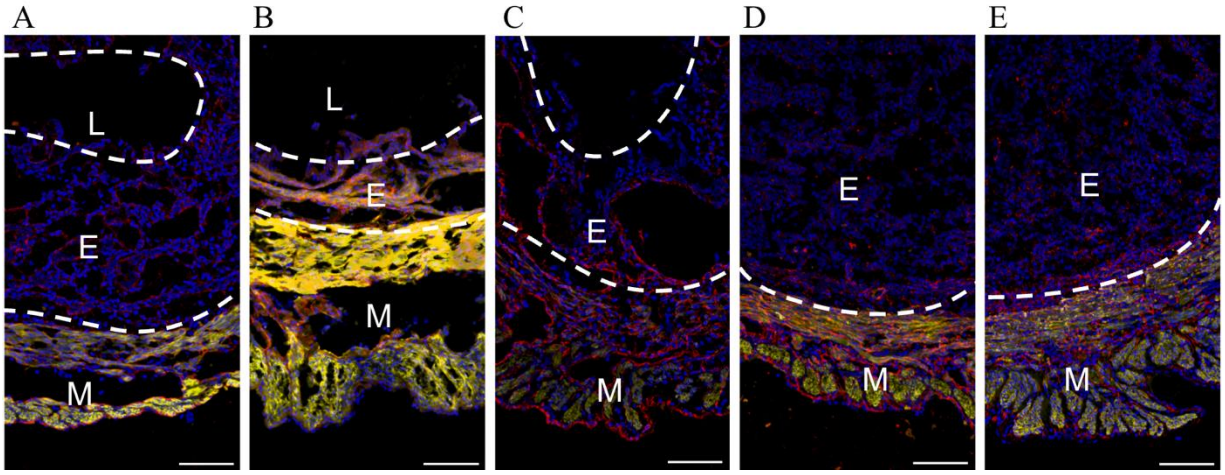

Figure 10: Representative immunofluorescence images from each postpartum time point, highlighting changes in the overall tissue's elastin (red) and smooth muscle cell (yellow) content. Immunofluorescent images of A) 8-week-old virgin uterine horn and uterine tissue at B) 1 day, C) 3 days, D) 7 days, and E) 14 days postpartum. Scale bars are 100 µm. (M = Myometrium, E = Endometrium, L = Lumen)

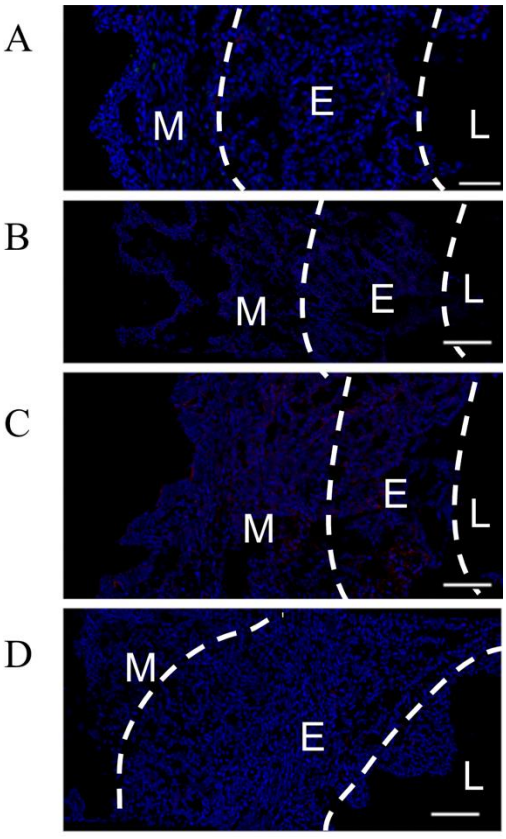

Figure 11: Representative histological images from each time point, highlighting changes in the overall tissue's macrophage (red) content. Immunofluorescent images of A) 8-week-old virgin uterine horn and uterine tissue at B) 1 day, C) 3 days, D) 7 days, and E) 14 days postpartum. (M = Myometrium, E = Endometrium, L = Lumen). Scale bars are 100 µm. (M = Myometrium, E = Endometrium, L = Lumen)

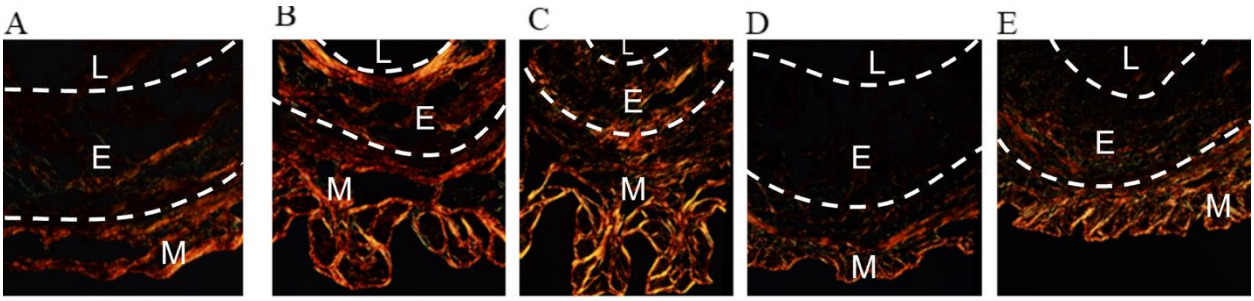

Figure 12: Representative histological images from each time point, highlighting changes in the overall tissue's collagen cell content. Birefringence images of A) 8-week-old virgin uterine horn and uterine tissue at B) 1 day, C) 3 days, D) 7 days, and E) 14 days postpartum. (M = Myometrium, E = Endometrium, L = Lumen)

Postpartum involution also affects the uterine tissue response to applied uniaxial loads. As shown in Figure 13A, postpartum uterine tissue can withstand loads almost twice as large as the virgin tissue at one day postpartum. A similar response is exhibited 3 days postpartum. However, over the course of involution, there is a drastic decrease in the force needed to rupture the tissue, with the 7 day postpartum and 14 day postpartum tissue failing at approximately 0.5 N and 0.4 N respectively. This is reduced relative to the non-pregnant control tissue. The resulting Cauchy stress, shown in **Figure 13C**, is trending lower at one day postpartum when compared to the control. At three days postpartum, there is a trend toward an increased stress response, but after 7 days postpartum, the stress the tissue can withstand returns to levels similar to the control. This phenomenon is especially highlighted in the tissue's stress-stretch response at 0.5 N, shown in **Figure 13F**. The tissue's ability to withstand deformations resulting from the applied loads remains relatively constant throughout involution, with the biggest change being at 14 days postpartum. Throughout involution, the level of strain the tissue can withstand and its ability to stretch in the face of applied loads varies slightly. However, as shown in **Figure 13D and 13E**, the tissue has the larger strain response, highlighting that postpartum involution alters the tissue biomechanical response to applied deformations.

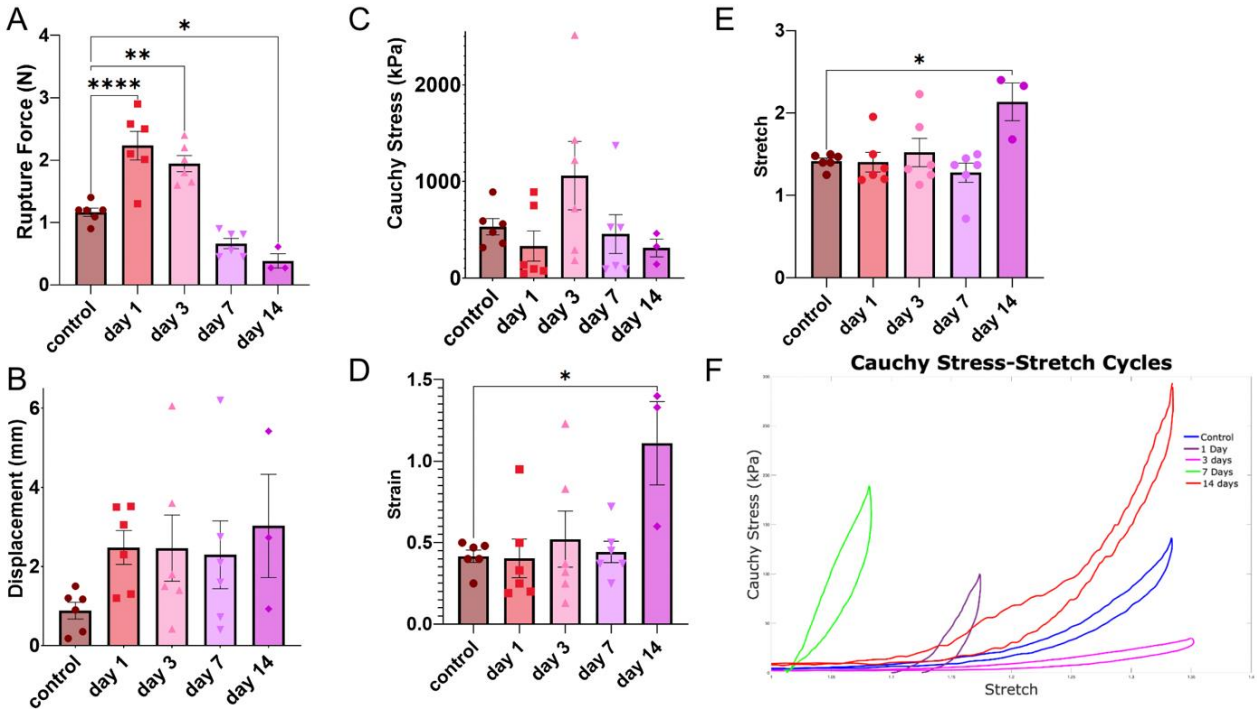

Figure 13: Uniaxial biomechanical analysis of postpartum murine uterine tissue showing changes in A) maximum rupture force, B) maximum displacement, C) Cauchy stress at failure, D) engineering strain at failure, and E) stretch at failure. F) Representative comparison of the control, 1 day, 3 day, 7 day, and 14 day postpartum Cauchy Stress-Stretch behavior as it is loaded to 0.5 N. * $p < 0.05$; one-way ANOVA with post-hoc Dunnett comparison to control

Overall, both the hysterotomy procedure and postpartum involution alter the biomechanics and resulting microstructure of murine uterine tissue.

Chapter 4: Discussion

The findings presented in this study provide comprehensive insights into the biomechanical alterations and microstructural changes that occur in murine uterine tissue following hysterotomy procedures and during postpartum involution.

Following hysterotomy procedures, our analysis revealed significant changes in uterine tissue microstructure over time. Tomographic images captured at different intervals post-hysterotomy demonstrated the progressive closure of the incision site, indicating ongoing tissue remodeling. Correspondingly, immunohistological images displayed alterations in cellular composition, with observable differences in cell distribution and density between injured and uninjured tissue. Changes in the smooth muscle cell, elastin and collagen content affect the overall biomechanical response of murine uterine tissue. Studies have found that an increase in collagen content, as observed in the uterine tissue at 2 and 3 weeks post-hysterotomy, can lead to an increase in the amount of stress the tissue is able to withstand[25]. Smooth muscle cells also influence the tissue's response to tensile loads. They play a crucial role in uterine contractility, extracellular matrix synthesis, and tissue plasticity[23]. Changes in the presence of these cells over the course of remodeling highlight their role in overall tissue integrity and elasticity. Studies have shown that the first two weeks following the hysterotomy procedure, and resulting remodeling of the myometrium, ultimately increases the stiffness and elasticity, but decrease in the overall strength of murine uterine tissue[22]. This manifests in lower rupture forces, Cauchy stresses, and strains when compared to the uninjured tissue. Macrophage infiltration also plays a prominent role in the early stages of wound healing, gradually decreasing as tissue remodeling progressed. By initiating the inflammation phase of wound healing and aiding in the overall development and repair of a wound, these cells help return the tissue to homeostasis[24]. Through their promotion of proliferation

and tissue formation, the decrease in their presence in three weeks post-hysterotomy demonstrates their value in restoring the tissue's integrity. These microstructural changes, highlighted by the changes in collagen, smooth muscle cell, elastin, and macrophage content, were paralleled in the changes observed in biomechanical properties. Initially, the injured tissue exhibited reduced strength and increased susceptibility to rupture compared to uninjured tissue, reflecting the early stages of wound healing. However, as the tissue underwent remodeling, its strength gradually increased, ultimately approaching levels comparable to uninjured tissue. The variations in stress-strain responses and rupture forces over tissue remodeling underscore the importance of tissue architecture on its biomechanical response.

Similarly, postpartum involution induced notable modifications in uterine tissue structure and biomechanical properties. Tomographic and immunohistological imaging revealed dynamic changes in tissue composition, including alterations in vascularization, elastin content, smooth muscle density, and immune cell infiltration during involution. Smooth muscle cells in the myometrium, along with collagenase and other proteolytic enzymes, contribute to this process by compressing the blood vessels, thereby restoring the tissue to its pre-pregnancy size[11]. Accelerating the autolysis process and inducing infarction of uterine blood vessels also reduces the overall size of the organ[13]. This is highlighted by the change in the size of the myometrium and difference in elastin and collagen content in both the endometrium and myometrium throughout involution. These changes were accompanied by fluctuations in tissue response to mechanical loading, with varying rupture forces and stress-strain characteristics observed at different stages of postpartum recovery. Notably, early postpartum tissue exhibited heightened resistance to rupture, potentially attributed to increased smooth muscle density and elastin content. However,

as involution progressed, tissue strength gradually declined, reaching levels below those of uninjured tissue.

While this study provides initial insights into biomechanical and microstructural changes that occur in murine uterine tissue following hysterotomy procedures and during postpartum involution, there are several limitations. With regards to mechanical testing, the defined testing procedure was considered to be a uniaxial state of loading. However, due to the nature of the samples geometry, the Cauchy stress and other biomechanical properties were determine using a pure shear analysis. Additionally, this work highlights the role of smooth muscle cells, collagen, elastin, and macrophages in tissue remodeling and biomechanical response. While these factors are undoubtedly important, their individual contributions and interactions within the complex tissue environment are not fully elucidated. Further research investigating specific cellular mechanisms and signaling pathways could enhance our understanding of uterine tissue remodeling.

The animal model used may also influence the results collected. For the hysterotomy procedure, longitudinal incisions were made to accommodate the size of the murine uterus. Conversely, transverse incisions are preferred in Cesarean sections to minimize blood loss and the risk of uterine rupture. The use of longitudinal incisions may affect the process of scar remodeling and the resulting biomechanics and structure of the tissue. Further research is necessary to comprehend the ramifications of employing each type of incision in this animal model. In our postpartum involution model, there was no control over the number of pregnancies and pups each animal had before sacrifice, which could influence the microarchitecture and biomechanical response measured during our testing. Future investigations should delve deeper into the birthing history of the animals utilized.

One mechanism that could be influencing remodeling is the estrous cycle. This process is the result of multiple remodeling events that help support ovulation and gestation[26]. These remodeling events lead to changes in uterine tissue thickness, reduced rate in luminal epithelial proliferation, and a decrease in luminal, glandular, and stromal apoptosis as a response to different steroidal environments[26]. By performing the hysterotomy at the same stage in the estrous cycle for each animal, we would be able to gain a deeper understanding as to what microstructural changes are the result of involution, scar remodeling, or estrous cycling.

Also, this research mainly uses imaging techniques like tomography and immunohistology to assess tissue microstructure. While these methods offer valuable information, they may not fully capture the dynamic nature of tissue remodeling and biomechanical changes. Future studies incorporating advanced imaging modalities or in vivo assessments could provide a more comprehensive understanding of uterine tissue behavior.

Finally, this study focuses on murine uterine tissue, which may not entirely represent the complexities of human uterine tissue physiology and response to injury. Murine models may exhibit differences in wound healing processes and tissue remodeling compared to humans. Additionally, while the study provides key insights into the effect of these remodeling processes on the murine tissue's biomechanical response, the translation of these findings to clinical practice requires further validation in human subjects.

Chapter 5: Conclusions and Future Works

By utilizing ex-vivo mechanical testing alongside noninvasive imaging techniques to explore the relationship between uterine scar morphology, postpartum involution, and the strength of uterine tissue against rupture, we were able to characterize the structural and biomechanical aspects of the mouse uterus during two different remodeling processes. The observed alterations in tissue biomechanics and microstructure underscore the intricate interplay between physiological processes and mechanical properties in uterine tissue.

Our findings contribute to a deeper understanding of how surgical interventions and postpartum physiological changes impact uterine health and function. Moreover, these insights may inform the development of strategies to optimize clinical interventions, such as enhancing wound healing or preventing postpartum complications. Future studies may further explore the biomechanical response the tissue experiences in response to biaxial loading. While this study focuses on tensile loading, this procedure may not fully reflect the diverse mechanical stresses experienced by uterine tissue during childbirth and postpartum recovery. Including a wider range of mechanical loading conditions could offer a more nuanced understanding of tissue behavior. Changes in the overall presence of TFG-β, vasculature, and other extracellular matrix components should also be explored to provide a greater context for the biomechanical changes observed.

This study also provides a framework for developing a model for studying uterine rupture. The impact of repeated involution and microstructural changes on the integrity of uterine scars and the biomechanical properties of the uterine wall remains unclear. Particularly, the compromised structural integrity around uterine scars poses significant risks in subsequent pregnancies, potentially resulting in severe delivery complications like uterine rupture, which can have grave consequences for both maternal and fetal well-being. By performing the hysterotomy procedure on both nonpregnant and pregnant mice and allowing that injury to heal, this animal model could be used to further explore the mechanics behind uterine rupture and scar remodeling. Additionally, this biomechanical assessment of the tissue could also be connected to a noninvasive imaging technique, such as MR imaging, thus helping to better define one's risk for uterine rupture. Understanding the gestational patterns in uterine scar remodeling based on thickness has proven challenging using traditional ultrasound imaging techniques. These findings imply that solely considering uterine geometry is insufficient, highlighting the necessity for innovative methods to non-invasively evaluate the risk of uterine rupture. This work serves as a promising initial framework for developing that tool.

Overall, in harnessing a comparative approach, this thesis illuminates the mechanical characteristics of uterine tissue throughout the postpartum healing process and scar remodeling. Through the two main objectives, the study characterizes the structural and biomechanical aspects of the mouse uterus during these two conditions, further emphasizing the correlation between the extent of uterine scar regeneration, involution, and tensile strength. Through the evaluation of mechanical properties of mouse uterine tissue in various remodeling conditions under tensile loading, this research provides potential insights into the clinical management and prevention of childbirth complications, especially in women with a history of C-sections.

References

1. Al-Zirqi I, Stray-Pedersen B, Forsén L, Vangen S. Uterine rupture after previous caesarean section. BJOG 2010;117:809–820.

2. Mark B. Landon, Predicting Uterine Rupture in Women Undergoing Trial of Labor After Prior Cesarean Delivery, Seminars in Perinatology, Volume 34, Issue 4, 2010, Pages 267-271, ISSN 0146-0005, https://doi.org/10.1053/j.semperi.2010.03.005.

3. Ameer, M. A., Fagan, S. E., Sosa-Stanley, J. N., et al. (2022, December 6). Anatomy, Abdomen and Pelvis: Uterus. In: StatPearls [Internet]. Treasure Island (FL): StatPearls Publishing. Available from: https://www.ncbi.nlm.nih.gov/books/NBK470297/

4. Gasner, A., & P A A. (2023, July 30). Physiology, Uterus. In: StatPearls [Internet]. Treasure Island (FL): StatPearls Publishing. Available from: https://www.ncbi.nlm.nih.gov/books/NBK557575/

5. Osol, G., & Mandala, M. (2009). Maternal uterine vascular remodeling during pregnancy. *Physiology (Bethesda, Md.), 24*, 58–71 [https://doi.org/10.1152/physiol.00033.2008] https://doi.org/10.1152/physiol.00033.2008

6. Meyer, N., & Zenclussen, A. C. (2020). Immune Cells in the Uterine Remodeling: Are They the Target of Endocrine Disrupting Chemicals? *Frontiers in immunology, 11*, 246. https://doi.org/10.3389/fimmu.2020.00246

7. Kiracofe, G. H. (1980). Uterine involution: Its role in regulating postpartum intervals. *Journal of Animal Science, 51*(suppl_II), 16–28. https://doi.org/10.2527/1980.51Supplement_II16x

8. Kristoschek, J. H., Moreira de Sá, R. A., Silva, F. C. D., & Vellarde, G. C. (2017). Ultrasonographic Evaluation of Uterine Involution in the Early Puerperium. *Revista brasileira de ginecologia e obstetricia : revista da Federacao Brasileira das Sociedades de Ginecologia e Obstetricia, 39*(4), 149–154. https://doi.org/10.1055/s-0037-1601418

9. Camilleri, C., Buskmiller, C., & Sammut, S. (2021). Pregnancy-induced long-term uterine vascular remodeling in the rat. *Reproductive Biology, 21*(1), 100466. https://doi.org/10.1016/j.repbio.2020.100466

10. Dessouky, A. D. (1971). Myometrial changes in postpartum uterine involution. *American Journal of Obstetrics and Gynecology, 110*(3), 318–329. https://doi.org/10.1016/0002-9378(71)90721-6

11. Cleveland Clinic. (n.d.). Uterus Involution. Retrieved from https://my.clevelandclinic.org/health/diseases/22655-uterus-involution

12. Mayo Clinic. (n.d.). C-Section. Retrieved from https://www.mayoclinic.org/tests-procedures/c-section/about/pac-20393655#:~:text=The%20more%20C%2Dsections%2C%20the,delivery%20in%20a%20later%20pregnancy

13. Chauhan, G., & Tadi, P. (2022, November 14). Physiology, Postpartum Changes. In: StatPearls [Internet]. Treasure Island (FL): StatPearls Publishing. Available from: https://www.ncbi.nlm.nih.gov/books/NBK555904/

14. Sung, S., & Mahdy, H. (2023, July 9). Cesarean Section. In: StatPearls [Internet]. Treasure Island (FL): StatPearls Publishing. Available from: https://www.ncbi.nlm.nih.gov/books/NBK546707/

15. Stupak, A., Kondracka, A., Fronczek, A., & Kwaśniewska, A. (2021). Scar Tissue after a Cesarean Section-The Management of Different Complications in Pregnant Women. *International journal of environmental research and public health, 18*(22), 11998. https://doi.org/10.3390/ijerph182211998

16. Scott, A. K., Louwagie, E. M., & Myers, K. M. (2023). bioRxiv 2023.11.03.565565. https://doi.org/10.1101/2023.11.03.565565

17. Togioka, B. M., & Tonismae, T. (2023, July 29). Uterine Rupture. In: StatPearls [Internet]. Treasure Island (FL): StatPearls Publishing. Available from: https://www.ncbi.nlm.nih.gov/books/NBK559209/

18. American College of Obstetricians and Gynecologists. (2017). Practice Bulletin No. 184: Vaginal Birth After Cesarean Delivery. *Obstetrics and gynecology, 130*(5), e217–e233. https://doi.org/10.1097/AOG.0000000000002398

19. Ratajczak, C. K., & Muglia, L. J. (2008). Insights into parturition biology from genetically altered mice. *Pediatr Res, 64*(6), 581–589.

20. Jayyosi, C., Lee, N., Willcockson, A., Nallasamy, S., Mahendroo, M., and Myers, K., 2018, “The mechanical response of the mouse cervix to tensile cyclic loading in term and preterm pregnancy,” Acta Biomaterialia, 18, pp. 308–319

21. McCarthy, R., Martin-Fairey, C., Sojka, D. K., Herzog, E. D., Jungheim, E. S., Stout, M. J., Fay, J. C., Mahendroo, M., Reese, J., Herington, J. L., Plosa, E. J., Shelton, E. L., & England, S. K. (2018). Mouse models of preterm birth: suggested assessment and reporting guidelines. *Biology of reproduction, 99*(5), 922–937. https://doi.org/10.1093/biolre/ioy109

22. Buhimschi, C. S., Zhao, G., Sora, N., Madri, J. A., & Buhimschi, I. A. (2010). Myometrial wound healing post-cesarean delivery in the MRL/MpJ mouse model of uterine scarring. *The American Journal of Pathology, 177*(1), 197-207. https://doi.org/10.2353/ajpath.2010.091209

23. Cao, R., Yang, Z. S., Hu, S. L., Liang, S. J., Zhang, S. M., Zhu, S. Q., Lu, L., Long, C. H., Yao, S. T., Ma, Y. J., & Liang, X. H. (2022). Molecular Mechanism of Mouse Uterine Smooth Muscle Regulation on Embryo Implantation. *International journal of molecular sciences, 23*(20), 12494. https://doi.org/10.3390/ijms232012494

24. Rodriguez, A., Tripurani, S. K., Burton, J. C., Clementi, C., Larina, I., & Pangas, S. A. (2016). SMAD Signaling Is Required for Structural Integrity of the Female Reproductive Tract and Uterine Function During Early Pregnancy in Mice. *Biology of Reproduction, 95*(2), 44(1–16). https://doi.org/10.1095/biolreprod.116.139477

25. Mondragon, E., Yoshida, K., & Meyers, K. (2013). Characterizing the biomechanical and biochemical properties of mouse uterine tissue. *Columbia Undergraduate Science Journal, 7*.

26. Bertolin, K., & Murphy, B. D. (2014). Reproductive Tract Changes During the Mouse Estrous Cycle. In B. A. Croy, A. T. Yamada, F. J. DeMayo, & S. L. Adamson (Eds.), *The Guide to Investigation of Mouse Pregnancy* (pp. 85-94). Academic Press. https://doi.org/10.1016/B978-0-12-394445-0.00007-2